Langmuir

ARTICLE

pubs.acs.org/Langmuir

Electrochemical Impedance Spectroscopy of Tethered Bilayer Membranes

Gintaras Valincius,*[,†] Tadas Meškauskas,[‡] and Feliksas Ivanauskas[‡]

[†]Vilnius University Institute of Biochemistry, Mokslininku 12, LT-08662 Vilnius, Lithuania

[‡]Vilnius University Faculty of Mathematics and Informatics, Naugarduko 24, LT-03225 Vilnius, Lithuania

Supporting Information

ABSTRACT: The electrochemical impedance spectra (EIS) of tethered bilayer membranes (tBLMs) were analyzed, and the analytical solution for the spectral response of membranes containing natural or artificially introduced defects was derived. The analysis carried out in this work shows that the EIS features of an individual membrane defect cannot be modeled by conventional electrical elements. The primary reason for this is the complex nature of impedance of the submembrane ionic reservoir separating the phospholipid layer and the solid support. We demonstrate that its EIS response, in the case of radially symmetric defects, is described by the Hankel functions of a complex variable. Therefore, neither the impedance of the submembrane reservoir nor the total impedance of tBLMs can be modeled using the conventional elements of the equivalent electrical circuits of interfaces. There are, however, some limiting cases in which the complexity of the EIS response of the submembrane space reduces. In the high frequency limit, the EIS response of a submembrane space that surrounds the defect transforms into a response of a constant phase element (CPE) with the exponent (α) value of 0.5. The onset of this transformation is, beside other parameters, dependent on the defect size. Large-sized defects push the frequency limit lower, therefore, the EIS spectra exhibiting CPE behavior with $\alpha \approx 0.5$, can serve as a diagnostic criterion for the presence of such defects. In the low frequency limit, the response is dependent on the density of the defects, and it transforms into the capacitive impedance if the area occupied by a defect is finite. The higher the defect density, the higher the frequency edge at which the onset of the capacitive behavior is observed. Consequently, the presented analysis provides practical tools to evaluate the defect density in tBLMs, which could be utilized in tBLM-based biosensor applications. Alternatively, if the parameters of the defects, e.g., ion channels, such as the diameter and the conductance are known, the EIS data analysis provides a possibility to estimate other physical parameters of the system, such as thickness of the submembrane reservoir and its conductance. Finally, current analysis demonstrates a possibility to discriminate between the situations, in which the membrane defects are evenly distributed or clustered on the surface of tBLMs. Such sensitivity of EIS could be used for elucidation of the mechanisms of interaction between the proteins and the membranes.

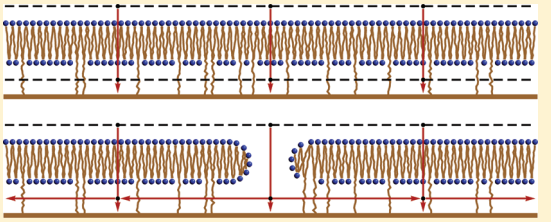

INTRODUCTION

Tethered bilayer membranes proposed by Lang et al.[1] constitute a class of biomimetic self-assembled structures that provide a generic platform for a broad spectrum of biophysical experiments such as peptide/membrane interactions,[2] protein/membrane interactions,[3] lipid phase transitions,[4] reconstitution of pore forming,[5] redox[6] and receptor[7] proteins, antigen/antibody binding,[8] and photocurrent generation.[9] Attached to a conducting surface, tBLMs allow monitoring of biologically relevant events with electrochemical techniques. One widely used technique is electrochemical impedance spectroscopy. EIS is an alternating current (ac) method, which probes surface electrodynamics in the frequency scale spanning typically from 10^{-3} to 10^{6} Hz. Some physical parameters, such as differential capacitance, solution resistance, and so forth, of the electrochemical system may be directly obtained from the electrochemical impedance (EI) spectra; however, the detailed physical information about the properties of interface is not directly accessible without modeling. One of the common ways to model EI spectra is based on the so-called equivalent electrical circuit (EEC). EEC models—typically constructed of electrical components, such as resistors, capacitors and, occasionally, other special elements—are designed to reproduce the EI spectral features and the parameters of the EEC elements then compared to the physical properties of the surface systems and processes.[10] There are numerous techniques to design EECs, however, most fall into two general approaches. The EEC may be assembled heuristically by comparing the experimental EI spectra to the model-generated one.[11,12] Alternatively, one may attempt the mathematical description of the electrical response of the system utilizing accessible structural and physical parameters.[13−15] For relatively simple systems—such as artificial black lipid membranes that consist of a planar dielectric sheet of phospholipid bilayer with no ion-transporters, protein channels, etc., and bathed from both sides by the electrolyte solution—the equivalent model can be derived by the first approach. The free-standing membrane model consists of a membrane capacitor C_m and a solution resistor R_s connected in series. Such a simple network generates the

Received: October 16, 2011
Revised: November 26, 2011
Published: November 29, 2011

Cole−Cole type EI spectra consistent with the experimental observations.[16] On the other hand, for complex geometries such as conducting nerve fibers[17] or planar membranes with ion-transporting components[13,14] the mathematical description of the systems is preferable because it allows one to describe the EI spectral features in the situations where no unique EEC model, containing simple electrical elements, can be derived.

Ideal tBLMs are relatively simple structures consisting of a series of homogeneous conductor/dielectric layers. In such a case, one may expect a series RC equivalent circuit to adequately model the EIS spectra as in the case of the black lipid membranes. Practically, it is unlikely that tBLMs will exhibit ideal geometry and homogeneity. Naturally occurring defects must be expected and their density directly related to the parameters of the formation process.[18] Spontaneous[19] or chemically induced[20] transient pores and the reconstitution of pore forming proteins and peptides also affect tBLM heterogeneity. Moreover, in contrast to free-standing black lipid membranes, the geometry of tBLMs is always asymmetric: the outer leaflet of the tBLM is bathed by an infinite (on the atomic scale) reservoir of the solution, while the inner leaflet is facing the constrained volume of the electrolyte, whose physical properties may be quite different compared to those in the solution bulk.[21] Such heterogeneous and geometrically asymmetric systems should exhibit specific EIS features that reflect the nature and the extent of tBLM heterogeneity.

EECs of different complexity have been proposed to account for the experimental features of the EI spectra of solid supported membranes.[11,22,23] Most of the suggested EEC models are heuristic by nature. The models satisfactorily reproduce spectral features of the tBLMs; however, the values of the EEC parameters are difficult to relate to the physical properties of the system. Characteristics such as "membrane resistance" and "membrane conductance" are frequently used;[24−26] however, the existing experimental data cast doubt as to whether such characteristics can be accessed directly from the EI spectra or from the EEC models. For example, the α-hemolysin induced membrane conductance of the tBLMs derived from the EEC systematically deviates from the conductance of the black lipid membranes.[26] Similarly, the EEC derived conductance of gramicidin-containing tBLMs did not exhibit ion selectivity as expected for the ion-selective gramicidin channels.[23] It was, therefore, argued that not only the conducting properties of proteins (defects) but also the geometry and the physical properties of the surface constructs, which includes the submembrane solution reservoir, may affect the EIS response of real tBLMs and the parameter values derived from the empiric EEC models.[21,26] To the best of our knowledge, the first attempt to account for these factors was carried out by Krishna et al.[21] who pointed out that the submembrane reservoir significantly affects the measured conductance of tBLMs and pointed out that the submembrane reservoir contribution may be modeled by 10 series ladder type RC elements forming a nonuniform distributed-parameter network. However, since this model was introduced heuristically and no fits of the experimental data to the model were presented, it is not clear whether this approach (a) adequately describes the EI spectral features, (b) can be used to retrieve physically relevant information from the spectra, such as the membrane defect density and size, or (c) may be used to predict spectral changes upon variation of the parameters of both the tBLM defects and geometry.

Scheme 1. Equivalent Electrical Circuit (EEC) Models of tBLMs[a]

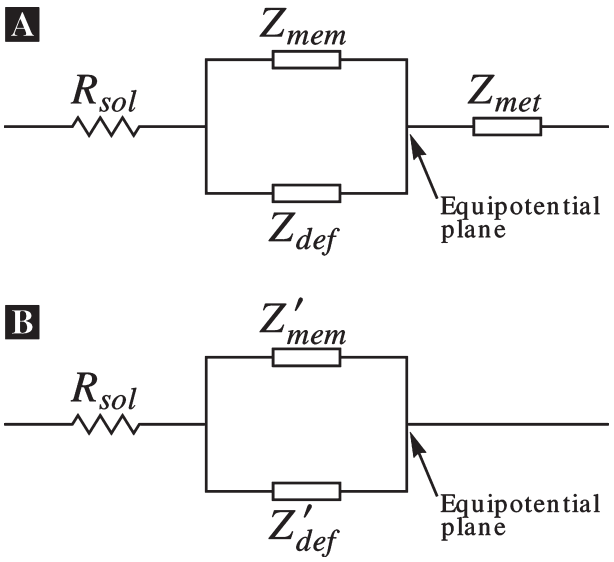

[a] (A) The commonly used[23] EEC presumes the equipotentiality of the space separating Helmholtz layer and the bilayer. This condition cannot be fulfilled in thin ionic reservoirs (1−2 nm) separating the phospholipid membrane from the solid support. (B) Alternative EEC which presumes equipotentiality of the metal solid support. This condition may be easily fulfilled using sufficiently thick metal layers.

This prompted us to search for a strict mathematical analysis that would allow modeling and prediction of EIS spectral features observed in tBLMs containing natural or artificially introduced defects: one in which the full analytical solution, if it exists, would both relate the physical parameters of tBLMs as well as determine whether or not tBLM EI spectra can be modeled by a unique EEC containing conventional electric elements.

FORMULATION OF THE PROBLEM

Scheme 1A shows the generic version of the commonly used EEC for tBLMs. The model consists of a solution resistance R_{sol} and three impedances: Z_{mem}, Z_{def}, and Z_{met}, the membrane, the defect, and the metal interface, respectively. Typically, in high concentration solutions containing no redox species, Z_{met} is considered an impedance Z_H of an ideal capacitor formed by the Helmholtz layer, i.e., $Z_{met} = Z_H = (j\omega C_H)^{-1}$. Here, $j = (-1)^{1/2}$, C_H is the Helmholtz layer capacitance, $\omega = 2\pi f$ is the cyclic frequency, and f is the ac frequency.

The circuit in Scheme 1A implies that the electric potentials U at all points along the metal|solution interface are equal, i.e., the space separating the Helmholtz layer and the bilayer membrane is equipotential. This condition is fulfilled only in ideal, defect-free tBLMs, as shown in Scheme 2A. In the absence of membrane defects, all electric field vectors are perpendicular to the surface and the potential values at all points in the submembrane space are equal, determined solely by the Helmholtz capacitance (C_H) and the capacitance of the bilayer membrane (C_m) (Note: Strictly speaking, the potential value is determined by the CPEs. CPE refers to an electrical element with an impedance, $Z_{CPE} = 1/(Q(j\omega)^{\alpha})$, where Q is the constant phase element coefficient, measured in Farads $\cdot cm^{-2} \cdot s^{\alpha-1}$, and the exponent α varies between 0 and 1. However, our experimental data show that the

dx.doi.org/10.1021/la204054g |Langmuir 2012, 28, 977–990

Scheme 2. Models of the tBLMs[a]

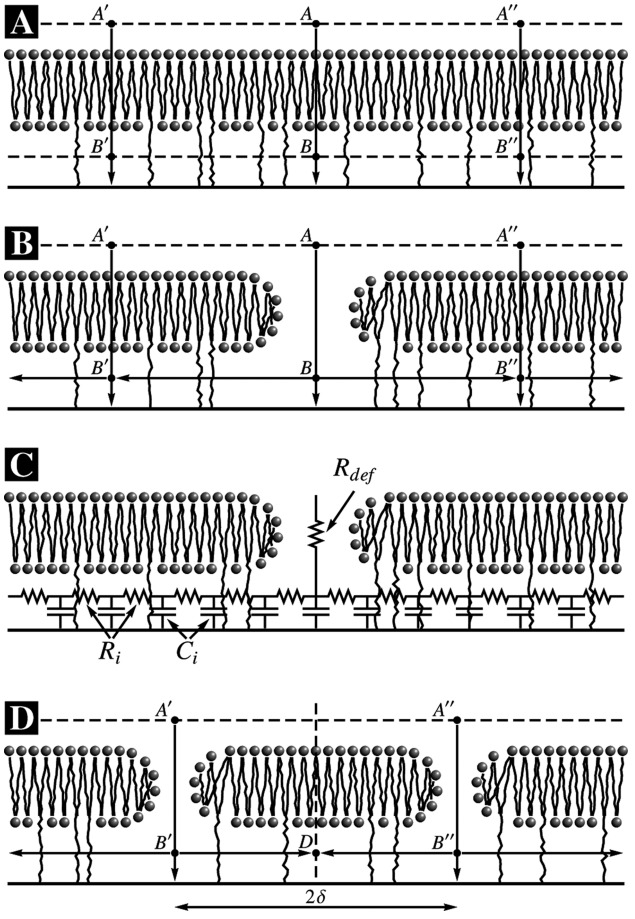

[a] (A) Cross section of the defect-free tBLM. (B) Cross section of the tBLM in the vicinity of a defect (electrolyte-filled pore). (C) Distributed network superimposed onto the tBLM model. In (A) and (B), arrows indicate the components of the electric field vectors and dashed horizontal lines indicate equipotential planes. In (C), R_i and C_i are the elements of the distributed-parameter network. (D) Cross section of the tBLM hosting two neighboring defects separated by a distance 2δ. Vertical dashed line marks the middle point between the two defects at which the components of the parallel to the surface electric field has same magnitude and opposed phases.

exponents of these CPEs are close to 1, so in this case, it is possible to approximate $C_H \approx Q_H$, and $C_m \approx Q_m$)

$$U_B \approx U_A \frac{C_m}{C_H + C_m}$$

However, in the presence of a defect, Scheme 2B, the electric field distribution changes and the equipotentiality of the submembrane space is no longer sustained. Because of the confined space and the limited mobility of ions populating the submembrane reservoir, the potential difference between points AB and points $A'B'$ and $A''B''$ are no longer equal, i.e., $U_B \neq U_{B'} = U_{B''}$. This gives rise to an electric field component parallel to a surface as is shown in Scheme 2B. The distance at which the defect-induced parallel component of the field will spread depends on the conductive properties of both the submembrane reservoir and the metal|reservoir interface. In addition to the perpendicular current flow across the bilayer membrane, an alternative defect-induced conductance pathway is created.

The EEC model in Scheme 1A is inconsistent with the electric field distribution (Scheme 2B) and must be replaced with an ECC containing two conducting pathways (Scheme 1B) and has an equipotential point located inside the metal. The equipotentiality in the metal phase is ensured by choosing a sufficiently thick layer of the metal support.

The EEC in Scheme 1B contains two impedances Z'_{mem} and Z'_{def} that characterize the impedance of the defect-free (membrane) and defect-populated segments on the tBLMs surface, respectively. The impedance Z'_{def} consists of two components: the impedance between points A and B (Scheme 2B), and the impedance between the points B and B' or B''. The former is the defect impedance Z_{def}, and the latter is the submembrane impedance Z_{sub}, i.e., $Z'_{def} = Z_{def} + Z_{sub}$. The impedances Z'_{mem}, Z_{def}, and Z_{sub} are determined by the dielectric properties of the phospholipid membrane, the size of the defect, the geometry, and the conductive properties of the submembrane space, as well as the Helmholtz layer.

For further consideration, we make the following assumptions: (a) the defect is a cylinder with radius r_0 and height d_{def}, (b) the phospholipid bilayer is separated from the solid support by a homogeneous electrolyte-filled reservoir of distance d_{sub}, (c) the specific resistance of the electrolyte in the reservoir is ρ_{sub}, and (d) the absence of any redox species in the system so that the impedance of the metal|reservoir interface is purely capacitive and is determined by the Helmholtz layer capacitance, C_H, which can be measured in a separate experiment in the absence of the tethered bilayer.[18] The resistive property of the submembrane reservoir, ρ_{sub}, is not directly accessible and can be only estimated based on the analysis of the EIS data. (There is experimental evidence that, due to the confined space between the metal and the hydrophilic head groups of the inner leaflet of the phospholipid bilayer and a lower dielectric constant, one may expect significantly lower ion mobility and, consequently, ionic conductance in the submembrane reservoir.[21]) Finally, we assume for the following analysis that the potentials of the outer tBLM surface, at the points A, A', and A'', are equal (Scheme 2B). This condition exists when the conductance of the solution is high and a proper (symmetrical) working-reference-auxiliary electrode configuration is chosen.

To find the impedance of the tBLM, we need to define the impedances Z'_{mem}, Z_{def}, and Z_{sub} that comprise the EEC model in Scheme 1B. The definition of Z'_{mem} and Z_{def} is straightforward because we assume ideally insulating properties of the phospholipid bilayer and purely resistive properties of the defect pore (Scheme 2B). However, Z_{sub} has never been analyzed analytically and its properties are not known. Therefore, we start with the problem of finding the impedance of the submembrane reservoir Z_{sub}, which manifests itself only when a tBLM defect is formed.

SUBMEMBRANE IMPEDANCE (ADMITTANCE)

Because of the finite conductance of the submembrane space and the nonzero capacitance of the Helmholtz layer, the electric field attenuates (Scheme 2B). To account for the attenuation, (assuming radial symmetry of field distribution) along the radial coordinate r, we introduce an infinite distributed-parameter network shown in Scheme 2C. The elements R_i and C_i of the network are

$$R_i = \bar{R}dr$$

$$C_i = \bar{C}dr$$

dx.doi.org/10.1021/la204054g |Langmuir 2012, 28, 977–990

where $\overline{R}$ and $\overline{C}$ are per unit length resistance and the capacitance of the network. R_i may be considered as the resistance of a hollow cylinder with the wall thickness of dr, while C_i is a planar ring-shaped capacitor with the inner ring radius r and outer ring radius $r + dr$. Both elements depend on the radial coordinate and are related to the physical parameters of the submembrane reservoir as follows:

$$\begin{cases} \overline{R} & = \dfrac{\rho_{sub}}{2\pi d_{sub}} \dfrac{1}{r} \\ \overline{C} & = 2\pi r C_H \end{cases} \tag{1}$$

where r is the radial distance (in cm), d_{sub} is the thickness (in cm), and ρ_{sub} is the specific resistance of the conducting media in the submembrane space (in $\Omega\cdot$cm), while C_H is the Helmholtz capacitance of a metal|reservoir interface (in F/cm^2).

Following de Levie,[27] we express the attenuation of the voltage along r as

$$dU = \frac{\partial U}{\partial r} dr = -i\overline{R} dr \tag{2}$$

and the ac current that enters the defect site is drained through the Helmholtz layer to the metal causing gradual attenuation of the current along r

$$di = \frac{\partial i}{\partial r} dr = -\overline{C} \frac{\partial U}{\partial t} dr \tag{3}$$

here t denotes time. Equations 2 and 3 could be rewritten as the system of differential equations

$$\frac{\partial U}{\partial r} + i\overline{R} = 0 \tag{4a}$$

$$\frac{\partial i}{\partial r} + \overline{C} \frac{\partial U}{\partial t} = 0 \tag{4b}$$

According to Dicker,[28] the analytical solution of the system of differential eqs 4a, 4b for nonuniform ($\overline{C}$ and $\overline{R}$ are functions of distance r) distributed-parameter network, in general, is not available. However, it is known that, for some electrochemical cases describing the electrochemical response for uniformly rough electrodes, in which $\overline{C}$ and $\overline{R}$ are the coordinate-dependent functions, analytical solution for eqs 4a, 4b can be obtained.[27]

Expressing the current i from eq 4a, and differentiating it with respect to r, one obtains the derivative $\partial i/\partial r$, which after substitution into eq 4b yields the differential equation

$$\frac{\partial^2 U}{\partial r^2} + \frac{1}{r}\frac{\partial U}{\partial r} - \frac{1}{k}\frac{\partial U}{\partial t} = 0 \tag{5}$$

in which $k = (\overline{R}\,\overline{C})^{-1} = d_{sub}/(\rho_{sub} C_H)$.

EIS techniques utilize the harmonic perturbation (voltage or current) of the system. This allows one to write the potential U as follows:

$$U = U_0 e^{j(\omega t + \varphi_u)} = \overline{u} e^{j\omega t} \tag{6}$$

where $\overline{u} = U_0 e^{j\varphi_u}$ is the phasor (complex amplitude) of the voltage. The phasor is time independent once the steady state is established. Assuming steady state condition, and by inserting U from eq 6 into eq 5, we obtain the differential equation containing no time argument

$$\frac{d^2\overline{u}}{dr^2} + \frac{1}{r}\frac{d\overline{u}}{dr} - j\frac{\omega}{k}\overline{u} = 0 \tag{7}$$

In eq 7, both the amplitude U_0 and the phase φ_u of $\overline{u}$ are the functions of the coordinate r and the cyclic frequency ω. The solution of eq 7 is only applicable to the steady state, in which the amplitude and the phase of U are constant.

The following study will involve the Hankel functions of the first kind $H_0^{(1)}(z)$, $H_1^{(1)}(z)$ (of the zeroth and the first order, respectively), and of the second kind $H_1^{(2)}(z)$, $H_1^{(2)}(z)$ (also of the zeroth and the first order, respectively), depending on the complex variable z (software for evaluation of the Hankel functions is listed in Supporting Information). The general solution of the differential eq 7 is[29]

$$\overline{u} = c_1 H_0^{(1)}(r,\omega) + c_2 H_0^{(2)}(r,\omega) \tag{8}$$

where c_1, c_2 are any constants, and the notations

$$H_n^{(m)}(r,\omega) = H_n^{(m)}\left(r(1-j)\sqrt{\frac{\omega}{2k}}\right) \tag{9}$$

are employed, here $m = 1, 2$ and $n = 0, 1$.

General expression for the current phasor $\overline{i}$ follows from eqs 8, 1, and 4a

$$\overline{i} = -\frac{2\pi d_{sub}}{\rho_{sub}} r \frac{d\overline{u}}{dr} \tag{10}$$

The derivative $d\overline{u}/dr$ (of the phasor $\overline{u}(r)$ of potential) which enters eq 10 is calculated taking into account the differentiation rules of the Hankel functions:[29]

$$\frac{d}{dz}H_0^{(1)}(z) = -H_1^{(1)}(z)$$
$$\frac{d}{dz}H_0^{(2)}(z) = -H_1^{(2)}(z)$$

Then, the general solution of the system of differential eqs 4a and 4b with respect to $\overline{i}(r)$ is

$$\overline{i} = (1-j)\pi C_H \sqrt{2\omega k}\, r \times \left[c_1 H_1^{(1)}(r,\omega) + c_2 H_1^{(2)}(r,\omega)\right] \tag{11}$$

The constants c_1, c_2 in eqs 8 and 11 must be determined by setting boundary conditions. One of these may be formulated for the point of entrance of ionic carriers into the submembrane space $r = r_0$ as follows:

$$\overline{u}(r_0) = U_0 \tag{12}$$

The second boundary condition can be formulated for two cases: (i) an infinite r interval (single defect) and (ii) a finite r interval (multiple defects). These cases are analyzed separately below.

SINGLE DEFECT IMPEDANCE (ADMITTANCE)

This condition corresponds to a situation with a single defect embedded in an infinite phospholipid bilayer. In such a case, the second boundary condition is

$$\overline{u}(r) \to 0, \quad r \to \infty \tag{13}$$

According to ref 29, $\lim_{r\to\infty}|H_0^{(1)}(r,\omega)| \to \infty$ and $\lim_{r\to\infty}|H_0^{(2)}(r,\omega)| \to \infty$. Therefore, it follows from eq 8 that $c_1 = 0$ and

$$c_2 = \frac{U_0}{H_0^{(2)}(r_0,\omega)}$$

dx.doi.org/10.1021/la204054g |Langmuir 2012, 28, 977–990

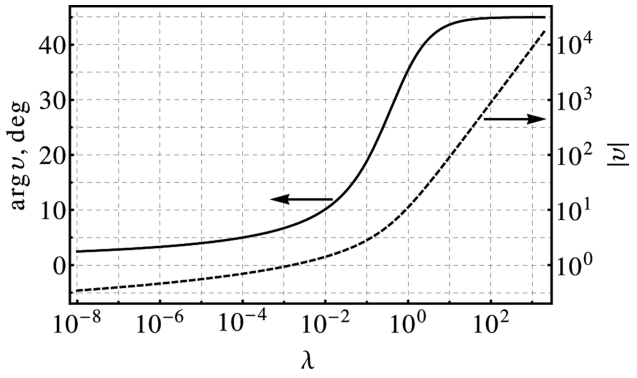

Figure 1. Dimensionless submembrane admittance υ (of a defect embedded into the infinite phospholipid bilayer) versus dimensionless frequency λ. Dashed curve is the magnitude $|\upsilon|$ of conductance; solid curve is the phase arg υ of conductance.

Putting c_1 and c_2 into eq 8, one obtains the following equation for voltage phasor:

$$\overline{u}(r) = U_0 \frac{H_0^{(2)}(r,\omega)}{H_0^{(2)}(r_0,\omega)} \tag{14}$$

Analogously, by employing 11, one finds the expression for the current phasor

$$\overline{i}(r) = U_0(1-j)\pi C_H\sqrt{2\omega k}\, r \frac{H_1^{(2)}(r,\omega)}{H_0^{(2)}(r_0,\omega)} \tag{15}$$

Even though eqs 14 and 15 allow estimating potential and current distribution in the submembrane reservoir along the coordinate r, from the practical standpoint, the value of the current at r_0 is important. Introducing the dimensionless frequency λ

$$\lambda = r_0\sqrt{\frac{\omega}{2k}} \tag{16}$$

(for the formula of the constant k, see eq 5), one obtains the expression for the electric current at r_0

$$\overline{i}(r_0) = U_0(1-j)2\pi \frac{d_{sub}}{\rho_{sub}} \lambda F(\lambda) \tag{17}$$

where the complex function $F(\lambda)$ is defined as

$$F(\lambda) = \frac{H_1^{(2)}\left((1-j)\lambda\right)}{H_0^{(2)}\left((1-j)\lambda\right)} \tag{18}$$

Thus, the dimensionless submembrane admittance υ is

$$\upsilon = \rho_{sub}\frac{\overline{i}(r_0)}{U_0 d_{sub}} = (1-j)2\pi\lambda F(\lambda) \tag{19}$$

Figure 1 plots the magnitude and phase of the dimensionless admittance as a function of a frequency. It exhibits two distinct regions. In the low frequency range, the admittance and its phase slowly trend toward zero, while in the high frequency range, above $\lambda \approx 1$, the admittance begins increasing with its phase trending arg $\upsilon \rightarrow \pi/4$. The analysis of the $\lambda F(\lambda)$ product (see Supporting Information) shows that

$$\upsilon \sim (1+j)2\pi\lambda + \pi, \quad \lambda \rightarrow \infty \tag{20}$$

As seen from eq 20, the magnitude of the admittance is linear with λ and, in turn (see eq 16), the complex conductance of the submembrane layer scales linearly with $\sqrt{\omega}$. Consequently, in the high frequency range, the impedance of the submembrane layer can be approximated by the CPE with the exponent $\alpha \approx 0.5$. This means the impedance of the submembrane starts behaving as the well-known Warburg impedance, which accounts for diffusion limited processes at electrodes.[30,31] However, despite the similarity to the Warburg impedance, the physical phenomena behind the features of the submembrane reservoir impedance are different.

To estimate whether the $\alpha \approx 0.5$ behavior manifests itself on measured EIS plots in accessible frequency ranges, real physical parameters must be put into eq 16. From eq 16, the onset point, $\lambda \approx 1$, depends on (i) the size of the defect r_0 and (ii) the physical properties of the submembrane space: d_{sub}, ρ_{sub}, and C_H, which enter into the constant k; see eq 5. The Helmholtz capacitance, C_H, value can be expected to be close to the capacitance of the anchor self-assembled monolayer (SAM) and can be measured separately. Our earlier data[2,18] and data obtained by others[32] show that the capacitance of sparsely populated anchoring SAMs is typically within the range from 5 to 10 μF/cm^2, while for anchor SAMs rich in cholesterol functional groups, the values are typically $\sim$3 μF/cm^2.[33] We assume the value $C_H = 10\,\mu$F/cm^2 for further modeling.

Submembrane layer thicknesses of tBLMs were estimated from neutron reflectometry.[18,26,32,34] Depending on the molecular composition of the anchor, it ranged from $\sim$1.3 to 2.1 nm. For further numerical estimates we will use the value d_{sub} = 1.6 nm.[35] In practice, both d_{sub} and C_H may be assumed to be constant; however, one needs to take into account that these properties are sensitive to the density of the tethered SAM[18] and the potential across the interface.[36] Less is known about the conductance of the submembrane resistance. A comprehensive study addressing this issue was carried out,[21] which showed from the EIS data analysis that the specific resistance in the submembrane space may be at least 3 orders of the magnitude higher in comparison to the specific resistance of the solution bathing the tBLMs. This is primarily because of the significantly lower ionic mobilities and the depressed dielectric constant in the constrained space between the solid electrode and the bilayer.

Substituting the above values of the physical parameters and varying values for r_0 and ρ_{sub} into eq 16, one obtains the $f_{\lambda=1}$ values at which the onset of the constant phase element behavior with $\alpha \approx 0.5$ starts to manifest itself in the EIS spectra of tBLMs containing isolated defects (Table 1). The estimates show that small (1−100 nm) radius defects and low specific resistance of the submembrane ionic reservoir ($\sim 10^2$−10^3 Ω·cm) exhibit CPE features with $\alpha \approx 0.5$ in the frequency range well above those typically accessible by EIS, i.e., f > 500 kHz (bold cells in Table 1). However, if the defect radius is large (>100−1000 nm) and/or the specific resistance of the submembrane reservoir is high ($\sim 10^3$−10^5 Ω·cm), the features of the CPE element with $\alpha \approx 0.5$[18,26] are noticeable in the EI spectra at experimentally accessible frequencies, e.g., from 0.5 Hz to 50 kHz. Supported by the data in Table 1, we argue that, in our earlier work,[18] in which the CPE with $\alpha \approx 0.5$ was observed in the frequency range at or below $\sim$200 Hz, the specific resistance of the submembrane space in tBLMs, prepared using the synthetic thiolipid tethers WC14[2,18,26,34] and FC16,[32] should fall into the interval from 10^4 to 10^5 Ω·cm, in qualitative agreement with the data in ref 21, and the residual defects

Table 1. Frequency $f\lambda$ in Hz at which the Submembrane Admittance (Impedance) Starts Exhibiting CPE Properties with $\alpha \approx 0.5$[a]

	specific resistance of the submembrane reservoir ρ_{sub}, Ω · cm			
defect size r_0, nm	10^2	10^3	10^4	10^5
1	**5.09×10^9**	**5.09×10^8**	**5.09×10^7**	**5.09×10^6**
10	**5.09×10^7**	**5.09×10^6**	**5.09×10^5**	5.09×10^4
100	**5.09×10^5**	5.09×10^4	5.09×10^3	5.09×10^2
1000	5.09×10^3	5.09×10^2	5.09×10^1	5.09×10^0

[a] The parameters of the submembrane reservoir: d_{sub} = 1.6 nm, C_H = 10 μF/cm^2. Cells in bold mark the frequency ranges not accessible for typical EIS measurements.

giving rise to a CPE behavior are scattered, relatively large (>100−1000 nm) tBLM uncovered patches.

In contrast, at $\lambda < 1$, the admittance (impedance) of the submembrane layer can be approximated by neither the CPE element nor any other simple electric equivalent. The phase (Figure 1) continuously trends down and, in the limit $\lambda \to 0$, the submembrane conductance (impedance) becomes resistive with an arg $\upsilon \to 0$ (also, see Supporting Information for the mathematical proof). However, the asymptotic expansion of the product $\lambda F(\lambda)$ in eq 19 approaches the limit

$$\lim_{\lambda \to 0} \upsilon = 0$$

which is equivalent to infinite impedance (open circuit) at $\lambda \to 0$.

Figure 1 shows that below $\lambda \lesssim 10^{-1}$, the submembrane admittance phase change is relatively slow. In such a situation, it is quite possible that the EIS curve can still be formally approximated by the CPE; however, the observed quasi-CPE will exhibit exponent values $\alpha < 0.5$. Although satisfactory fits could be obtained with the equivalent circuits containing CPEs with $\alpha < 0.5$,[32] both the coefficient and the exponent of the CPE lack physical meaning and may not be used to retrieve physical parameters of the tBLM system.

An unrestricted increase of the submembrane thickness leads to a geometry similar to that of the black lipid membranes. As follows from eq 16, an increase of the parameter d_{sub} leads to a decrease of λ, which is followed by arg $\upsilon \to 0$. However, the current at r_0 (see eq 17), and the admittance of the submembrane, increases to infinity with d_{sub}. At some point, being totally resistive, it will surpass the admittance of the defect, $Y_{def} = Z_{def}^{-1}$, whose properties do not depend on d_{sub}. Such a situation is electrically equivalent to the black lipid membrane system, in which a single defect in the membrane is surrounded by highly conducting media from both sides.

IMPEDANCE (ADMITTANCE) OF MULTIPLE DEFECTS

In real systems the situations with single isolated defects are unlikely. There will always be a finite number of defects scattered across the interface, which, at higher densities, may electrically interact with each other due to their proximity. Initially we address the condition of evenly distributed, maximally packed defects and then (*vide infra*) we discuss the possible consequences of the more realistic situation of heterogeneity of defect distribution. Homogenously distributed defects in membrane surfaces must exhibit thermal lateral mobility. For proteins, this requires the phospholipid membrane to be separated from the supporting surface,[37] as is achieved with tBLMs.

We now seek a solution of eq 7 for the finite interval of r. To account for finite densities of defects, we introduce a defect occupancy radius δ, which defines the area $S_{def} = \pi\delta^2$ of a circle that hosts a circular defect with radius r_0 in its center. For evenly distributed maximally packed defects, δ equals half the distance between two neighboring defects (Scheme 2D); the area occupied by a defect is $S_{def} \approx \pi\delta^2/0.907$ and the defect density is defined as $N_{def} \approx 0.907/(\pi\delta^2)$. The highest possible density of the arrangement of equal radius circles on a two-dimensional plane is $\pi/\sqrt{(12)} \approx 0.907$.

The solution of eq 7 requires setting boundary conditions. The first boundary condition is the same as in the infinite r case and is defined by eq 12, i.e., at the point of the entrance of the electric flux into the submembrane space $r = r_0$, $\overline{u}(r_0) = U_0$. Another boundary condition sets the current phasor value to

$$\overline{i}(\delta) = 0 \tag{21}$$

at $r = \delta$. The condition in eq 21 reflects the fact that the radial components of the current vectors, at the point $r = \delta$ (Scheme 2D), from two adjacent defects due to a symmetry of the arrangement of defects are equal in magnitude and have the opposite phases. This assumption allows us to significantly simplify the problem, keeping it one-dimensional. Strict analysis would require the formulation of at least a two-dimensional problem, which would include an additional space variable that would account for the lateral heterogeneity of the current distribution. This simplification only marginally affects both the qualitative and quantitative conclusions of the current analysis as long as we consider evenly distributed defects. From eq 15, the current phasor decays exponentially as $r \to \infty$, so at sufficiently large distance from r_0, the current magnitude tends to 0, and the simplification is well-justified. However, we note that, at large r_0/δ ratios, e.g., $r_0/\delta > 0.3$, the condition in eq 21 may no longer be applicable for all points with $r = \delta$. Consequently, the model presented in this work may not be applicable to describe the EIS response of the high defect density tBLMs. Another problem arises from the fact that the interstices between the circles with radius δ are not accounted for in the following analysis. This will result in an undervaluation of the low frequency conductance of the submembrane by up to ~10% (*vide infra*).

Applying the boundary conditions eqs 12 and 21 to eqs 8 and 11, one obtains the expression for the current phasor:

$$\overline{i}(r) = U_0(1-j)\pi C_H\sqrt{2\omega k}\, r \times \frac{H_1^{(2)}(\delta,\omega)H_1^{(1)}(r,\omega) - H_1^{(1)}(\delta,\omega)H_1^{(2)}(r,\omega)}{H_1^{(2)}(\delta,\omega)H_0^{(1)}(r_0,\omega) - H_1^{(1)}(\delta,\omega)H_0^{(2)}(r_0,\omega)}$$

By defining the dimensionless defect domain radius as $L = \delta/r_0$, we obtain the compact expression for the dimensionless conductance of the submembrane reservoir between the point of the entrance $r = r_0$ and the electrode

$$\upsilon = \rho_{sub}\frac{\overline{i}(r_0)}{U_0 d_{sub}} = (1-j)2\pi\lambda H(\lambda) \tag{22}$$

dx.doi.org/10.1021/la204054g |*Langmuir* 2012, 28, 977–990

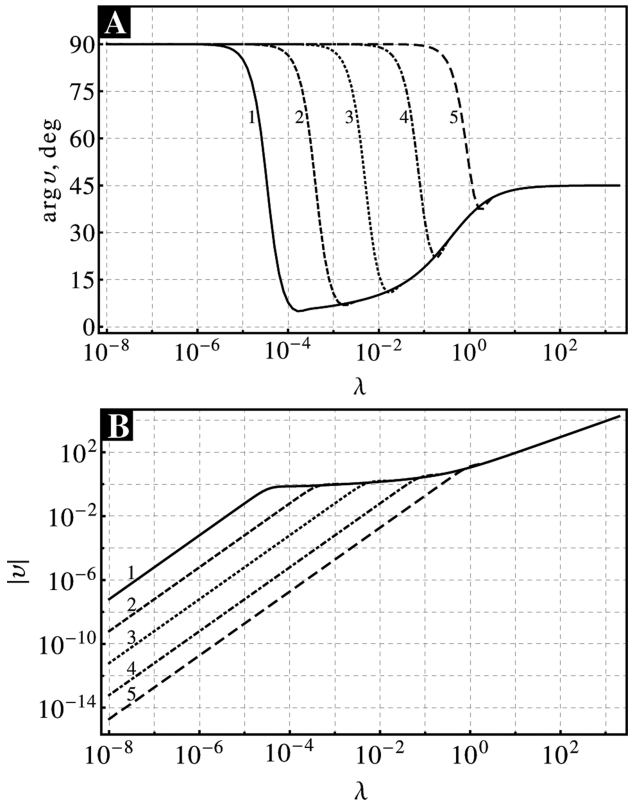

Figure 2. Spectra of the dimensionless submembrane admittance phase arg υ (A) and the magnitude $|\upsilon|$ (B) at different defect densities. Dimensionless defect domain radius $L = \delta/r_0$, curves: 1, 10^4; 2, 10^3; 3, 10^2; 4, 10; 5, 2.

in which the complex function $H(\lambda)$ is

$$H(\lambda) = \frac{H_1^{(2)}(L\Lambda)H_1^{(1)}(\Lambda) - H_1^{(1)}(L\Lambda)H_1^{(2)}(\Lambda)}{H_1^{(2)}(L\Lambda)H_0^{(1)}(\Lambda) - H_1^{(1)}(L\Lambda)H_0^{(2)}(\Lambda)} \qquad (23)$$

here $\Lambda = (1 - j)\lambda$ and the dimensionless frequency λ is defined by eq 16.

Figure 2 displays the spectra of the phase (Figure 2A) and magnitude (Figure 2B) of the dimensionless admittance υ at different defect densities (dimensionless parameter L). In the high frequency range ($\lambda > 1$), the admittance of the defect surrounded by other defects is identical to the admittance of a single isolated defect, because eq 22 at $\lambda > 1$ transforms into eq 20. Consequently, the admittance of the submembrane space starts exhibiting a constant phase element behavior with the argument arg $\upsilon \rightarrow \pi/4$. Physically this means that increasing the frequency leads to the electrical isolation of the defects. This happens because the electric field component along the coordinate r decays fast and essentially vanishes at the boundary δ. Therefore, at high frequencies, the electrical response of the membrane defect in the presence and in the absence of the neighbor defects becomes indistinguishable. Consequently, high frequency parts of the submembrane impedance can be modeled by the CPE with $\alpha = 0.5$.

However, in the low frequency range, the admittance of the submembrane space in tBLMs containing multiple nonisolated defects differs from that in tBLMs with isolated defects (compare Figure 1 and Figure 2). In the low frequency range (the limit of the frequency range now depends on L), the admittance phase

Scheme 3. Generic Equivalent Electric Circuit of the tBLM[a]

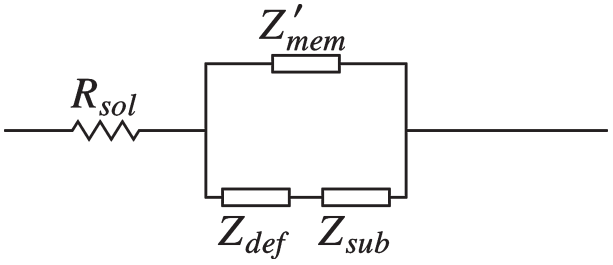

[a] Z'_{mem} is the impedance related to the phospholipid membrane capacitance; it also includes contribution from the Helmholtz capacitance. Z_{sub} is the submembrane space impedance which may be calculated from eq 22, and Z_{def} is the membrane defect impedance, which depends on the nature of the defect.

quickly trends toward arg $\upsilon \rightarrow \pi/2$, instead of approaching 0, while its magnitude exhibits quadratic dependence from λ. It can be demonstrated (see Supporting Information) that, at $\lambda \rightarrow 0$, eq 22 transforms into the following expression:

$$\upsilon \sim 2\pi j(L^2 - 1)\lambda^2 \qquad (24)$$

The latter taking into account the definitions of L and λ can be transformed into the expression for the submembrane admittance Y_{sub}

$$Y_{sub} = Z_{sub}{}^{-1} = \frac{d_{sub}}{\rho_{sub}}\upsilon \qquad (25)$$

where υ is defined by eq 22. Then, as $\lambda \rightarrow 0$,

$$Y_{sub} \sim j\omega\pi(\delta^2 - r_0^2)C_H \qquad (26)$$

Equation 26 shows that at low frequencies the submembrane reservoir admittance is an admittance of an electrical capacitor, whose parameters are solely determined by the Helmholtz capacitance and defect size (Note: Interstices between the circles with radius δ are not accounted for in the current analysis; therefore, the value of the conductance is undervalued in eq 26 by ~10%. In the final expression for the electrode impedance, this undervaluation diminishes the value of the Helmholtz capacitance by ~4−6%).

TOTAL IMPEDANCE OF tBLMS

Once the submembrane admittance Y_{sub} (impedance, Z_{sub}) is defined, we may now design the EEC for the total impedance of the tBLM. The generic, two conductance pathways EEC is shown in Scheme 3. It consists of solution resistance, R_{sol}, and Z'_{mem}, Z_{def}, and Z_{sub}, which are correspondingly the membrane, the defect, and the submembrane impedances that are dependent on the electrical properties of the phospholipid membrane and the defect.

The total impedance of the circuit shown in Scheme 3 is

$$Z_{tot} = R_{sol} + \frac{1}{N_{def}} \frac{1}{(Z'_{mem})^{-1} + (Z_{def} + Z_{sub})^{-1}} \qquad (27)$$

In eq 27, R_{sol} is the total solution resistance of one cm^2 of the surface area, while the impedances Z'_{mem}, Z_{def}, and Z_{sub} are per one defect. The coefficient $1/N_{def}$ takes into account defect density; consequently, the second member of the sum in eq 27 is the tBLM impedance of one cm^2 area. To calculate the total

dx.doi.org/10.1021/la204054g |Langmuir 2012, 28, 977–990

impedance of the electrode covered by the tBLM, one needs to define Z'_{mem}, Z_{def}, and Z_{sub} in eq 27. Z_{sub} is calculated according to eq 25.

The membrane impedance (Scheme 3) is capacitive in nature, and is defined as follows:

$$Z'_{mem} = \frac{1}{j\omega C_{mH}} \quad (28)$$

Here C_{mH} is dependent on both the phospholipid bilayer and Helmholtz capacitances and is defined as

$$C_{mH} = (C_m^{-1} + C_H^{-1})^{-1}\pi(\delta^2 - r_0^2) + C_H\pi r_0^2 \quad (29)$$

where the phospholipid membrane capacitance is

$$C_m = \frac{\varepsilon_m\varepsilon_0}{h_m} \quad (30)$$

and ε_m, ε_0 are the dielectric constant and the vacuum dielectric constant, respectively, while h_m is the thickness of the dielectric sheet of the bilayer.

The definition of Z_{def} depends on the nature of the defect. In this paper we restrict the analysis to the case in which the defect is an electrolyte-filled membrane spanning pore. Consequently, the defect impedance is purely ohmic in nature. It is a resistor, $Z_{def} = R_{def}$, whose magnitude is determined by the geometry of the pore and the solution properties inside it.

The following analysis could be extended to other heterogeneous systems, such as those formed by cholesterol rafts, with purely capacitive properties or systems that involve complex ion translocation through the membrane mechanisms.[13] However, these more complex cases are outside the scope of the current work.

MEMBRANE SPANNING PORES

As seen from Scheme 3, the defect branch of the total impedance is determined by the sum of the impedances $Z_{def} + Z_{sub}$. Which of these dominates depends on the properties of the submembrane and the defect itself. The conductance of water-filled ion channels covers a wide range from several[38−40] to several hundreds[41] of thousands of picosiemens (pS).[42,43] The conductance of the submembrane layer can be calculated from eqs 22 and 23, taking into account eq 16 and the definition of the parameter L as $L = \delta/r_0$.

The conductance $Y_{sub} = Z_{sub}^{-1}$ of the 1.6 nm thick submembrane created by a 1 nm size pore is plotted as a function of frequency f (in Hz) in Figure 3. In the frequency range from ∼1 to ∼1000 Hz at $N_{def} = 0.3\ \mu m^{-2}$, and from ∼10 to ∼1000 Hz at $N_{def} = 30\ \mu m^{-2}$, the submembrane conductance exhibits a relatively flat region. This is the region in which typical EI spectral changes induced by the protein−membrane interactions are observed.[23,26] From Figure 3, it follows that membrane spanning pores with $R_{def}^{-1} < 10$ pS will dominate in the defect branch of the impedance (Scheme 3) if the submembrane conductance $\rho_{sub} = 10^4\ \Omega\cdot$cm. This condition changes to $R_{def}^{-1} < 1$ pS if the submembrane conductance is $\rho_{sub} = 10^5\ \Omega\cdot$cm. Thus, whether or not the conductive properties of the membrane spanning pores are accessible from the EIS data analysis depends primarily on the specific resistance of the submembrane reservoir and, for $\rho_{sub} = 10^4$−$10^5\ \Omega\cdot$cm, even relatively large, water-filled membrane nanopores, such as the heptameric channel formed by α-hemolysin (α-HL; single channel conductance is ∼90 pS in 0.1 M NaCl),[44]

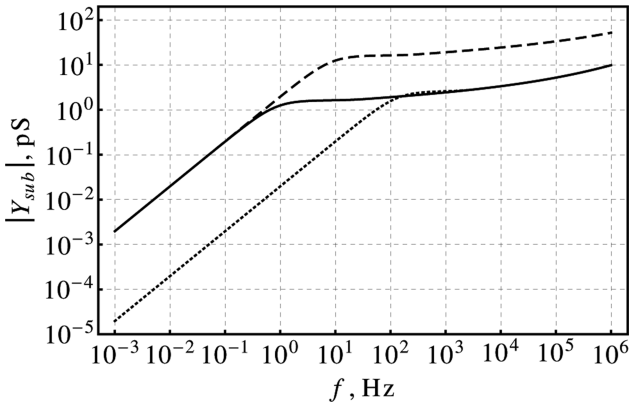

Figure 3. Conductance of the submembrane reservoir created by a single 1 nm ($r_0 = 10^{-7}$ cm) radius defect. Submembrane reservoir parameters: $C_H = 10^{-5}$ F/cm^2, $d_{sub} = 1.6$ nm, solid and dotted curves, $\rho_{sub} = 10^5\ \Omega\cdot$cm; dashed curve, $\rho_{sub} = 10^4\ \Omega\cdot$cm. Density of defects: solid and dashed curves, $N_{def} = 0.3\ \mu m^{-2}$, dotted curve, $N_{def} = 30\ \mu m^{-2}$.

should at least partially contribute to the defect branch of the tBLM impedance. The available experimental data support this conclusion. For example, the conductivity of the α-HL pore may be modulated by nonionic polymers.[26,45,46] In 30% aqueous solution of PEG 1000 (w/w), the conductivity of the α-HL channel, reconstituted into freestanding black lipid membranes, decreases by ∼40% from its value in the polymer-free solution. Under the same conditions, the tBLM conductance change upon the introduction of PEG 2000 is significantly smaller and comprises only ∼10−12% of the initial value.[26] In another experiment,[23] the gramicidin-induced conductance exhibited no cationic specificity observed in black lipid experiments. This indicates that the gramicidin-induced conductivity of tBLMs measured by EIS does not reflect the intrinsic conductivity of the channel. The reason for smaller than expected variations of the EIS-derived conductivity changes is related to the fact that the defect induced conductivity pathway is dominated not by the conductance of defect but also primarily by the complex conductance of the submembrane layer.

Figure 4 demonstrates model EI spectra of tBLMs containing $r_0 = 1$ nm defects at ∼30 μm^{-2} density. The Bode plots contain typical features reflecting the presence of the defects (ion channels) in the tBLM. In particular, the impedance modulus, $|Z_{tot}|$, exhibits a step-like kink (Figure 4A) whose position coincides with the impedance phase, arg Z_{tot}, local maximum (local minimum of the −arg Z_{tot}, indicated by arrow in Figure 4B) at frequency f range 10−1000 Hz. Whether or not the value of the $|Z_{tot}|$ at frequency of the phase extremum reflects the intrinsic properties of the membrane pore depends on the conductance of defects as well as on the properties of the submembrane.[21,23]

The EIS curves in Figure 4 demonstrate that the intrinsic conductive properties of the defects do not manifest themselves in the EI spectra if their conductance is high. In this particular case, defects with conductance >10 pS (resistance <100 GΩ) exhibit indistinguishable EIS model spectra. The spectral features depend primarily on the properties of the submembrane layer rather than defect properties. When the single channel conductance is small (<10 pS), the features on both $|Z_{tot}|$ and arg Z_{tot} model plots start following changes in Z_{def}. The approximate condition that determines whether or not the intrinsic defect

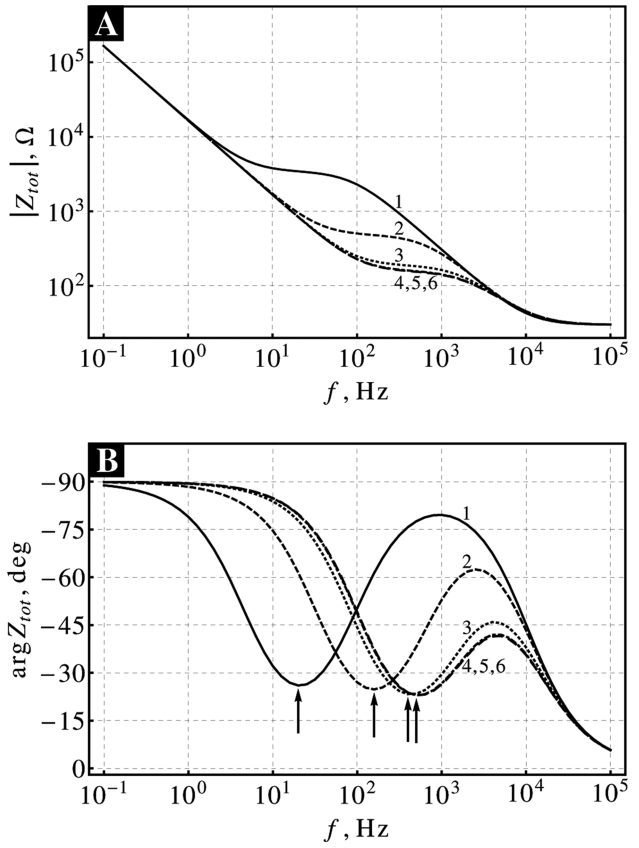

Figure 4. Model Bode plots of the total impedance of tBLMs containing ion channels (r_0 = 1 nm) of different conductance. Pane A: impedance magnitude, pane B: impedance phase. Submembrane reservoir parameters: $C_H = 10^{-5}$ F/cm^2, d_{sub} = 1.6 nm, $\rho_{sub} = 10^5$ Ω·cm. Phospholipid layer parameters are ε_m = 2.2, h_m = 3.2 nm, and vacuum permittivity $\varepsilon_0 = 8.85 \times 10^{-14}$ F/cm. Density of defects: N_{def} = 30 μm^{-2}. Single channel conductance $Y_{def} = Z_{def}^{-1}$, curves: 1, 0.1 pS; 2, 1 pS; 3, 10 pS; 4, 100 pS; 5, 1000 pS; 6, 10 000 pS. Spectra are calculated per 1 cm^2 of electrode surface, with solution resistance R_{sol} = 30 Ω·cm^2. Arrows point to local minimums of the functions −arg $Z_{tot}(f)$.

properties are "visible" in the EI spectra can be formulated as the thresholds determined by the following inequalities:

$$Z_{def} = R_{def} > 0.2\frac{\rho_{sub}}{d_{sub}} \quad (31)$$

or

$$Y_{def} = R_{def}^{-1} < 5\frac{d_{sub}}{\rho_{sub}} \quad (32)$$

where Y_{def} is the conductance of a single defect. Above the threshold determined by eq 31, or below the threshold determined by eq 32, the defect resistance starts dominating in the defect branch of the EEC (Figure 5), and the properties of the defect become accessible for the EIS.

The same conditions, eqs 31 and 32, apply also to Cole−Cole EI spectra, which represent the plot of imaginary vs real component of the complex capacitance of tBLMs

$$C_{tot} = \frac{1}{j2\pi f Z_{tot}}$$

Model Cole−Cole plots of different conductance defects in tBLMs are shown in Figure 5. The spectra exhibit a typical

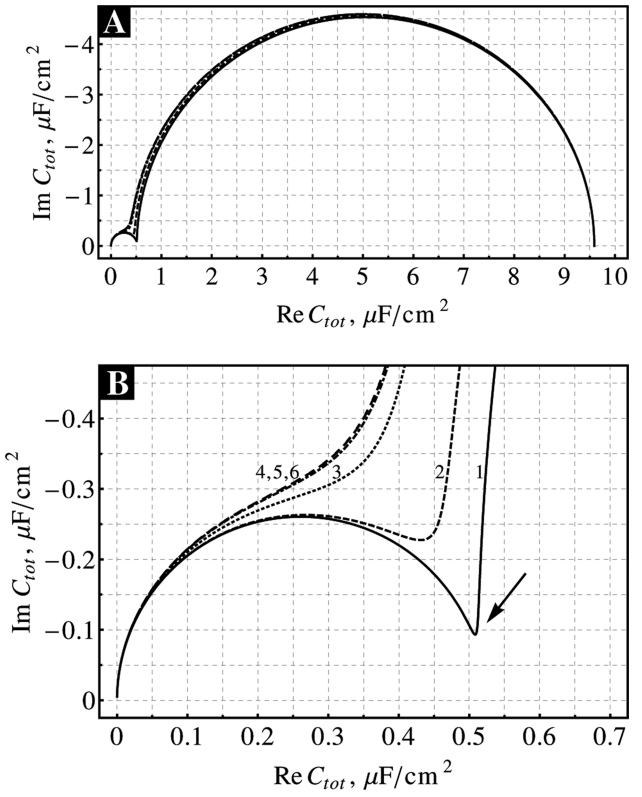

Figure 5. Model Cole−Cole plots of different conductance for ion channels (radius = 1 nm) reconstituted into the tBLM. Pane A: frequency range 10^{-4}−10^6 Hz, pane B: enlarged high-frequency part of the spectrum. The curves refer to the same conductivities Y_{def} (in pS) as in Figure 4. Submembrane reservoir parameters: $C_H = 10^{-5}$ F/cm^2, d_{sub} = 1.6 nm, $\rho_{sub} = 10^5$ Ω·cm. Phospholipid layer parameters are ε_m = 2.2, h_m = 3.2 nm, and vacuum permittivity $\varepsilon_0 = 8.85 \times 10^{-14}$ F/cm. Density of defects N_{def} = 30 μm^{-2}, solution resistance R_{sol} = 30 Ω·cm^2. Arrow indicates an extremum point on the plot that moves "northwest" as the intrinsic conductance of the defect increases.

"two semicircle" shape, characteristic of the presence of defects in tBLMs.[35] As in the Bode plots, these spectra are indistinguishable for the single channel conductances >10 pS (resistance <100 GΩ). Below 10 pS, the characteristic spectral feature, an extremum formed by the boundary between two semicircles (the transition from one to another occurs in the ∼50−500 Hz range, depending on the parameters of the system), moves "north and west" in the complex plane (ReC_{tot}, $-ImC_{tot}$) as the conductance of the individual membrane defect increases. Single channel conductance can be modulated artificially upon adding neutral polymers,[26,46,47] varying ionic composition,[48] bias voltage, or adding ligands[49,50] that trigger significant changes in pore conductance. Therefore, the "northwest" trajectory of the extremum (Figure 5), which is sensitive to the individual defect conductance, can be used as a diagnostic criterion of such variations. However, one must be cautious here because the position of the extremum is also affected by the submembrane resistance ρ_{sub} and, to a certain extent, by the resistance of the solution R_{sol}.

The spectral features described above were observed in real experiments. Figure 6 demonstrates the response of α-HL channels reconstituted in tBLMs to the addition of the nonionic polymer—polyethylene glycol PEG 1000 (average molecular weight 1000 Da). The PEG 1000 molecules are small enough to enter the α-HL channel. The polymer decreases single channel

dx.doi.org/10.1021/la204054g |*Langmuir* 2012, 28, 977−990

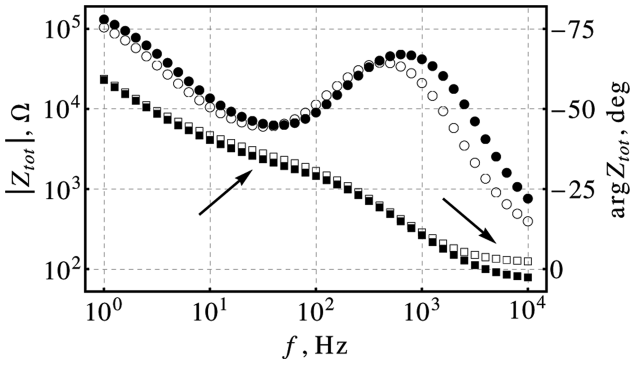

Figure 6. Experimental Bode spectra of diphytanoyl phosphocholine tBLMs with reconstituted α-HL channels. Squares, $|Z_{tot}|$; circles, arg Z_{tot}; filled symbols, curves obtained with no PEG 1000; open symbols, with 15% (w/w) PEG 1000 in solution. Reconstitution of protein was performed at 50 nM concentration of α-HL in 0.1 M KCl + 0.01 phosphate buffer at 7.5. After reconstitution, the electrochemical cell was flushed with copious amounts of buffer.

conductance by ~40%,[26,46] which is very close to the bulk conductance decrease in the solution containing 15% (w/w) PEG.

In Figure 6 the resistance increase upon PEG 1000 addition is most clearly visible in the high frequency ($f > 10^3$ Hz) part of the spectra where the resistance of the solution primarily determines Z_{tot} (spectral feature range denoted with the downward arrow). R_{sol} increases by a factor of ~1.7 and is consistent with the 40% decrease of the buffer bulk conductivity upon addition of 15% PEG 1000. However, less pronounced impedance changes are seen in the mid frequency range (spectral range denoted with the upward arrow). $|Z_{tot}|$ changes by only a factor of 1.17, less than expected for the 40% decrease of the conductance of an individual α-HL channel. Such effect may be observed in the situation as follows: (a) the PEG 1000 molecule is small enough to partition into α-HL pore, however, it is not capable of penetrating the submembrane space, and cannot alter its conductance, and (b) the single channel conductance is close to the boundary condition in eq 32; consequently, both the channel and the submembrane contribute comparably to the defect branch of the impedance Z_{tot}. This allows estimates of the submembrane resistance of tBLM systems for the experiment in Figure 6 (such tBLM systems were described earlier[26]); e.g., putting ~90 pS, the value for α-HL single channel conductance in 0.1 M KCl buffer at pH 7.0,[44] and d_{sub} = 1.6 nm, as determined from the neutron reflectometry,[18] into eq 32, one obtains $\rho_{sub} < 9\times 10^4$ Ω·cm for the specific resistance of the submembrane space. Assuming that ρ_{sub} is not far from this threshold, we conclude that $\rho_{sub} \approx (5-9) \times 10^4$ Ω·cm. This value is almost 3 orders in magnitude higher than the specific resistance of the bulk solution of 0.1 M KCl, consistent with earlier estimates made using finite element analysis[23] and modeling using ladder-type EECs.[21]

DENSITY OF THE MEMBRANE SPANNING PORES

For very low conductance pores ($Y_{def} < 1$ pS), the defect branch of EIS is determined by the properties of the membrane pore. In this case, the estimation of the membrane-spanning pore density is straightforward and can be found using the following ratio:

$$N_{def} \approx \frac{Z_{def}}{Z_{min}} \qquad (33)$$

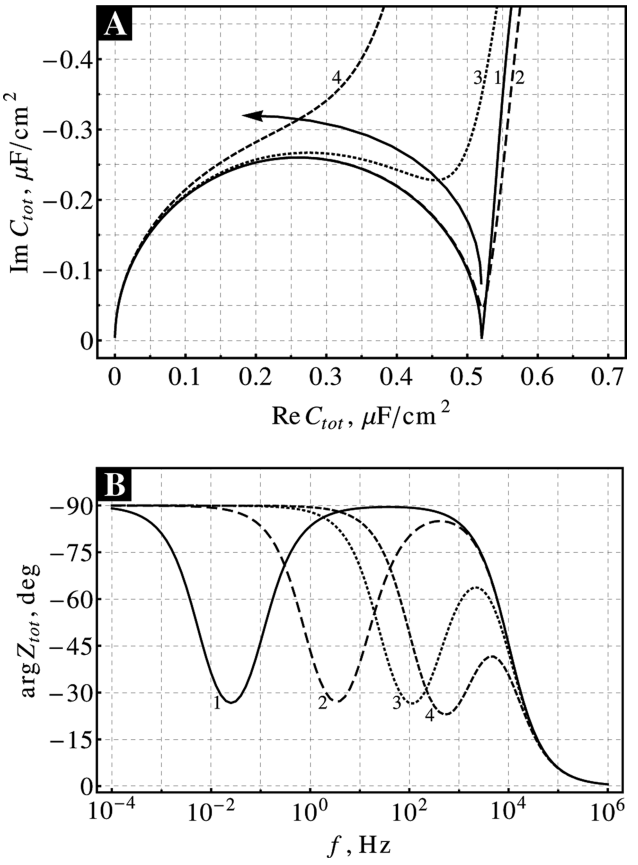

Figure 7. Cole−Cole (A) and Bode (B) plots of EI spectra for defects (r_0 = 1 nm) at different densities. Pore conductance $Y_{def} \approx$ 900 pS. Defect density N_{def}, curves: 1, 0.003 μm^{-2}; 2, 0.3 μm^{-2}; 3, 7.2 μm^{-2}; 4, 30 μm^{-2}. Arrow in (A) indicates the trajectory of the movement of the extremum point of the curve following the defect density increase. Other modeling parameters are R_{sol} = 30 Ω·cm^2, $C_H = 10^{-5}$ F/cm^2, d_{sub} = 1.6 nm, $\rho_{sub} = 10^5$ Ω·cm. Phospholipid layer parameters are ε_m = 2.2, h_m = 3.2 nm, and vacuum permittivity $\varepsilon_0 = 8.85 \times 10^{-14}$ F/cm.

Here Z_{min} is the electrode total impedance value at the frequency f_{min}, defined by the local minimum of the −arg $Z_{tot}(f)$.

Many protein pores exhibit single channel conductances well above 1 pS. For channels with Y_{def} > 100 pS, eq 33 cannot be used. Nevertheless, the analysis indicates that EI spectral features are extremely sensitive to the variation of the defect density despite the fact that, in such situations, the conductance of the submembrane space, not the conductance of the pore, dominates the defect branch of the impedance. This is illustrated by the Cole−Cole spectra in Figure 7A. The modeling shows that for hypothetical membrane pores (r_0 = 1 nm) increasing the defect density from 0.003 to 30 μm^{-2} results in significant changes in the complex capacitance plots. The semicircular part of the spectra, which corresponds to the high frequency edge of the curve, "lifts off" the x-axis and moves "northwest" in the complex plane. If this is observed in EIS Cole−Cole plots, it may be used as a diagnostic criterion of an increase in defect density. We note that such features will be observed only if the defects are distributed evenly across the tBLM (Scheme 4A). As we will show subsequently, this feature does not develop, in the case of defect clustering. The spectra in Figure 7A also demonstrate the extraordinary sensitivity of the EIS technique. Defect surface coverage, expressed as the ratio $(r_0/\delta)^2$, spans the interval from

Scheme 4. Schematics of the Distribution of Defects in tBLMs[a]

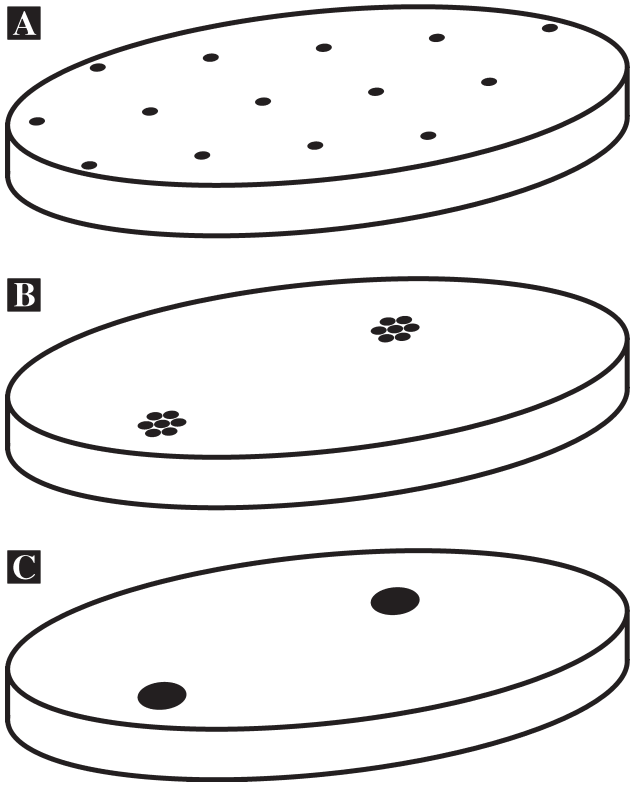

[a] A: evenly distributed small defects. B: clusters of small defects. C: larger defects with the radius equal to the radius of the cluster.

10^{-8} to 10^{-4}, as the surface defect concentrations increase from 0.003 to 30 μm^{-2}.

Defect densities can also be estimated by the minimum on the curve $-\arg Z_{tot}$ vs f. Figure 7B displays calculated EIS Bode plots of the membrane pores ($r_0 = 1$ nm) for defect densities N_{def} from 0.003 to 30 μm^{-2}. In this simulation, the conductance of an individual pore is set to $Y_{def} \approx 900$ pS (10-fold that of the α-HL channel in 0.1 M KCl). The phase minimum on the $-\arg Z_{tot}$ vs f plot moves from approximately 0.025 to 3.3 Hz as the defect density increases from 0.003 ($\delta = 10^{-3}$ cm) to 0.3 μm^{-2} ($\delta = 10^{-4}$ cm), and then to 516 Hz, as the defect density rises to 30 μm^{-2} ($\delta = 10^{-5}$ cm). Thus, the phase extremum frequency f_{min} changes roughly by one decade of f per 1 order of magnitude of N_{def}. The analysis indicates that N_{def} vs f_{min} plot on the log−log scale exhibits an almost linear trace with the local slope ≈0.93 as the defect density increases from 0.003 to 30 μm^{-2}. In this density range, the surface concentration of membrane pores can be approximately estimated using the following equation:

$$\lg N_{def} \approx 0.93 \lg f_{min} - \lg k - 0.2 \lg r_0 - \text{const} \qquad (34)$$

Here const = 1.24 is determined from the following parameters: $r_0 = 1$ nm, $k = 1.6 \times 10^{-7}$ cm²/s, $C_H = 10^{-5}$ F/cm², $R_{sol} = 30\ \Omega \cdot cm^2$, $\varepsilon_m = 2.2$, $h_m = 3.2$ nm, $\varepsilon_0 = 8.85 \times 10^{-14}$ F/cm. The constant in eq 34, in a strict mathematical sense, is not a constant, varying slightly with parameters, making the precision of the estimates based on eq 34 dependent on the N_{def} range. Table 2 summarizes the errors of estimates obtained using eq 34, compared to exact values (defined by the analytical expression eq 27).

Table 2. Relative Errors of Defect Density N_{def} Estimates Obtained Using eq 34 from Exact Values

Defect radius		Exact	Estimated	
r_0, nm	Frequency f_{min}, Hz	N_{def}, μm^{-2}	N_{def}, μm^{-2}	Relative error
1	516	2.89×10^{1}	3.02×10^{1}	4.5%
10	1090	2.89×10^{1}	3.81×10^{1}	32.1%
1	3.3	2.89×10^{-1}	2.72×10^{-1}	5.7%
10	5.02	2.89×10^{-1}	2.57×10^{-1}	11.0%
100	9.78	2.89×10^{-1}	3.01×10^{-1}	4.3%
1	0.0242	2.89×10^{-3}	2.83×10^{-3}	2.0%
10	0.0328	2.89×10^{-3}	2.39×10^{-3}	17.2%
100	0.0502	2.89×10^{-3}	2.26×10^{-3}	21.7%
1000	0.0976	2.89×10^{-3}	2.62×10^{-3}	9.3%

In some cases, errors are considerable, reaching 20−30%; however, taking into account the fact that the defect density estimates can be made for the interval spanning 4 orders of magnitude, one may consider the equation as a satisfactory approximation.

Equation 34 could be applicable to highly conducting protein pores such as human perforins,[51] cholesterol dependent cytolysins, and other large diameter protein channels. For such proteins, their pore size only weakly affects the EIS spectral features, in the functional manner determined by eq 34. In the case of intermediate size pores, neither eq 33 nor eq 34 can be applied. In such cases, one may consider modification of the physical properties of the tBLMs so that the conditions in eq 31 or eq 32 become applicable. Alternatively, one may apply fitting to the model algorithms using the analytical expression eq 27.

SIZE OF THE DEFECTS

In tBLMs, defect sizes may change in various ways. Processes may continuously increase the size of the bare surface area such as the enzymatic digestion of the phospholipid bilayer by phospholipases.[34] On the other hand, it is known that the membrane proteins may form clusters in the phospholipid bilayers.[52−55] Membrane pores formed by such proteins will tend to aggregate into entities (Scheme 4B), which will behave electrically as the continuous defects of the size of the formed cluster (Scheme 4C). This statement is strictly applicable to the systems for which the condition eq 32 is fulfilled, or the systems comprise clusters that significantly exceed in size the individual defect, or the distance between the individual defects is smaller or comparable to the defect radius.

First, we will estimate the impedance (conductance) of the membrane defects of various size, assuming they are water filled cylinders with the height equal to the thickness of the hydrophobic layer of the membrane, and cylinder radius r_0. The cylindrical pore is separated from the metal surface by the distance equal to thickness of the submembrane space, $d_{sub} = 1.6$ nm. The impedance Z_{def} of such a defect exhibits resistive properties and, therefore, can be modeled by the resistance R_{def}

$$R_{def} = \frac{\rho_{def}}{\pi r_0^2} d_{def} \qquad (35)$$

in which ρ_{def} is the specific resistance of the solution inside the pore and d_{def} is the length of the pore. If, due to thermal fluctuations, a pore spontaneously forms an opening in the membrane, e.g., a transient pore, then d_{def} is the thickness of the hydrophobic core of the membrane. If the membrane defect is

dx.doi.org/10.1021/la204054g |Langmuir 2012, 28, 977−990

Table 3. Resistance R_{def} and Conductance $Y_{def} = R_{def}^{-1}$ of the Various Size Defects Estimated by FEA[a]

Defect radius r_0, nm	Defect resistance R_{def} by FEA, Ω	Defect conductance Y_{def} by FEA, nS
1	1.13×10^9	0.88
10	2.45×10^7	40.82
100	2.13×10^6	469.48
1000	2.26×10^5	4424.78

[a] Physical parameters of a defect are d_{sub} = 1.6 nm, d_{def} = 3.2 nm, and ρ_{def} = 100 Ω·cm.

formed by a pore-forming protein, then d_{def} is the length of the water-filled channel inside the protein. Due to the complex interior structure and possible interaction of ions with the lumen surface, eq 35 based estimates, in most cases, will yield inaccurate values for small size protein pores. For example, the radius of the pore at the ends of an α-HL channel is about 1 nm, and the length of the protein is about 10 nm.[56] For such a 0.1 M KCl solution-filled cylinder, one may expect single channel conductance values from eq 35 to be ~300 pS, whereas the experimental values are ~90 pS.[44]

For larger pores, eq 35 becomes inapplicable for other reasons. The current lines in large pores concentrate along the perimeter of the defect and, in turn, their conductance should scale with r_0 (the perimeter) instead of r_0^2 (the area) as implicated by eq 35. Therefore, we conclude that eq 35 yields poor estimates of the conductance of the water filled defects.

The analytical solution of the current distribution in the vicinity of the defect is quite complex. Numerical finite element analysis (FEA)[35] may provide a less cumbersome way for evaluating the resistance (conductance) of such pores. The FEA problem was formulated earlier.[35] The results of the FEA modeling are summarized in Table 3. Based on the values in Table 3, one may derive the empirical equation for the resistance R_{def}, which, for r_0 ranging from 1 to 1000 nm, is

$$R_{def} = 10^{-(0.086x^3 + 1.25x^2 + 6.97x + 8.03)} \quad (36)$$

in which $x = \lg r_0$. In eq 36 r_0 is in centimeters, and R_{def} is in ohms. The practical utility of eq 36 is restricted to the set of parameters d_{sub}, d_{def}, and ρ_{def} indicated in Table 3 caption. For another set, one needs to redefine the coefficients in eq 36 by solving the Laplace equation by FEA.[35]

The resistance values from Table 3 were used to calculate the total impedance of the tBLM containing defects of different size. The calculated EIS spectra are shown in Figure 8. The defect size-related spectral changes predominantly occur in the low frequency part of the spectra. In contrast to the defect density increase, the defect size increase results in only marginal variations of the Bode plots (Figure 8A). The impedance phase minimum slowly shifts toward the high frequency range as the defect size increases. Comparison of the curves in Figure 7B and Figure 8A indicates that, even when the tBLM surface defect coverage is the same, e.g. $\sim 10^{-4}$, as is the case for the 30 μm^{-2} curve (Figure 7B) and the 100 nm curve (Figure 8A), the Bode curves exhibit their phase extremum at different frequencies, i.e., ~500 Hz and ~0.01 Hz, respectively. The corresponding Cole−Cole spectra also exhibit qualitative differences. In contrast to the defect density effect, the defect size increase results in a noticeable enlargement of the diameter of the high frequency semicircle (Figure 8B). At the same time, the mid frequency

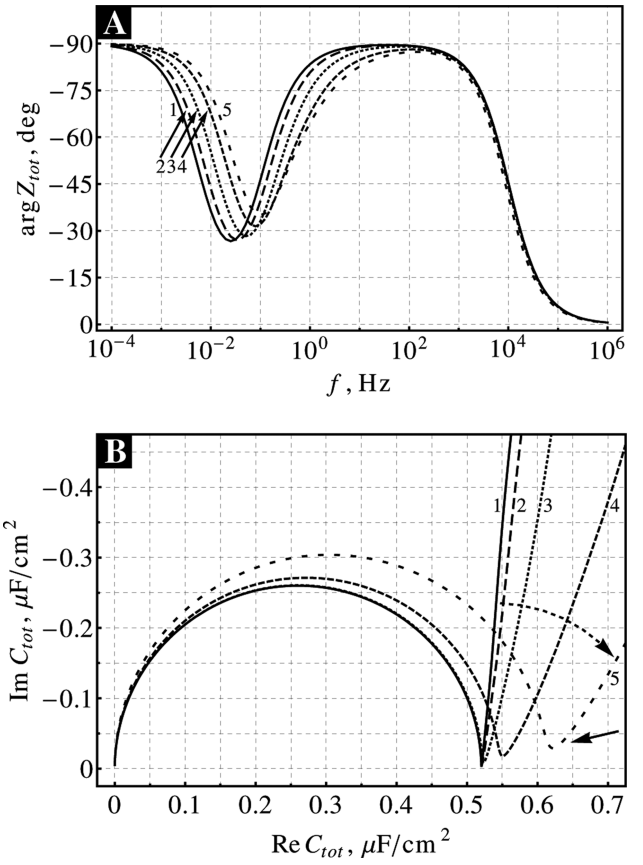

Figure 8. Bode (A) and Cole−Cole (B) plots of tBLMs containing different size defects. The radius of the defects r_0, curves 1, 1 nm; 2, 10 nm; 3, 100 nm; 4, 500 nm; 5, 1000 nm. The density of defects is N_{def} = 0.003 μm^{-2}. Other modeling parameters are R_{sol} = 30 Ω·cm^2, C_H = 10^{-5} F/cm^2, d_{sub} = 1.6 nm, ρ_{sub} = 10^5 Ω·cm. Phospholipid layer parameters are ε_m = 2.2, h_m = 3.2 nm, and vacuum permittivity ε_0 = 8.85 × 10^{-14} F/cm. Frequency ranges of the plots are from 1 MHz to ~0.1 Hz (for r_0 = 1 nm defects) and ~1 Hz (for r_0 = 1000 nm defects). Solid arrow in (B) indicates the characteristic extremum point of the curve that moves "northeast" as the size of the defects increases. Dashed arrow in (B) indicates change in the slope of the plots as the size of the defects increases.

extremum shown by the solid arrow in Figure 8B moves "northeast" in the complex Cole−Cole plane as the size of the defect increases. Such variations of the plots were observed in palmitoyl oleoyl phosphatidyl choline tBLMs upon their digestion by the phospholipase A_2.[34]

Another feature of the EIS spectra seen in Figure 8B is the slope of the curve changes (indicated by dashed arrow) with defect size after it passes through the extremum point. At constant defect density, small defects yield a curve slope of ~90 degrees (provided x- and y- axes are scaled identically), while large defects shift the slope toward 45°. This effect is directly related to the change of the submembrane impedance associated with the defect size. As the size of the defect increases, at λ = const, ω decreases (see eq 16). Consequently, the spectral range in which the submembrane impedance attains the phase value of 45° moves into the low frequency range, where it dominates the defect branch ($Z_{sub} \gg R_{def}$) and is not obscured by the impedance of the membrane ($Z_{sub} \ll Z_{mem}$). Most likely, the near 45° slopes observed in a number of experiments[18,32] on

dx.doi.org/10.1021/la204054g |Langmuir 2012, 28, 977–990

freshly prepared tBLMs arise from large defects present at low densities on the surface.

Because densely packed clusters are electrically similar to continuous defects, the differences in spectral features in Figure 7 and Figure 8 allow one to distinguish situations depicted in Scheme 4A and B, i.e., to detect and identify the formation of the clusters.

CONCLUSIONS

The analysis carried out in this work shows that the ac response of an individual membrane defect cannot be modeled by a unique set of electrical elements. Consequently, the impedance of tBLMs or any other surface supported insulating layers that bear an ionic conducting layer between the solid support and the layer cannot be modeled by equivalent circuits containing a finite number of simple electric elements such as capacitors (constant phase elements) and resistors. The reason for this is the complex nature of the submembrane reservoir impedance, comprising a nonhomogeneous distributed parameter network, for which the mathematical expressions eqs 19 and 22 were herein derived.

The mathematical analysis shows that in some limiting cases the EI response may be reduced to a finite set of conventional elements. In the high frequency limit, the submembrane impedance becomes the impedance of a CPE with the exponent $\alpha \approx 0.5$. In the low frequency limit, the response of one single defect becomes resistive ($\arg Z_{sub} \rightarrow 0$, though $Z_{sub} \rightarrow \infty$), while the response of the multiple defects becomes capacitive, i.e., $Z_{sub} \rightarrow j\omega C_H$, as was recently observed in tBLMs upon addition of gramicidin.[57]

The lateral density of water-filled channels in the membranes can be estimated from the analysis of the EI spectra. However, the methodology of the analysis depends on the ratio between the conductance of an individual channel and the conductance of the submembrane reservoir. For low conductance channels, their surface density may be directly assessed from the measured tBLM conductance. For highly conducting channels ($Y_{def} > 10$ pS), their surface density may be determined from the EIS data if the physical properties (specific resistance and thickness) of the submembrane reservoir are known. In this case, however, the empirical relations that link the EI spectral features (e.g., the frequency of the impedance phase extremum in the Bode plot) with the defect density, can be derived. Such relationships may be utilized in sensor applications, for example, in quantitative analysis of the activity of pore-forming toxins.

Our analysis demonstrates the possibilities of the EIS technique to identify cases in which the formation of defect clusters occurs. Cluster size and their surface density impacts the features of the EI spectra; consequently, such parameters may in principle be extracted from the experimental EIS plots.

Finally, even though our analysis was carried out for tBLM systems, the formalism presented in this work may be easily extended to other solid supported objects. They must contain defects and be composed of two layers with significantly different electrical conductances: the higher conductance layer must be facing a solid support and the lower conductance layer facing the electrolyte. Such systems would involve self-assembled monolayers formed by the organic compounds containing molecular segments of different hydrophobicity,[58,59] hybrid bilayer systems,[60] free-floating supported monolayers[61] and bilayers,[62] and polymer cushion supported bilayer[63] systems.

ASSOCIATED CONTENT

Supporting Information. Mathematical limits of the Hankel functions and software for their evaluation. This material is available free of charge via the Internet at http://pubs.acs.org.

AUTHOR INFORMATION

Corresponding Author

*E-mail: gintaras.valincius@bchi.vu.lt. Phone: +370-52720186. Fax: +370-52729196.

ACKNOWLEDGMENT

This work was supported by the Research Council of Lithuania "IMFAbite" project (grant agreement No. MIP-096/2011). Fruitful discussions with D. J. Vanderah (Institute for Bioscience and Biotechnology Research, University of Maryland), J. Robertson and J. J. Kasianowicz (National Institute of Standards and Technology, Gaithersburg, MD), R. Budvytyte and M. Mickevicius (Vilnius University) are greatly acknowledged. G. V. thanks for the financial support provided by the University of Maryland and the National Institute of Standards and Technology for visits and access to their research facilities.

REFERENCES

(1) Lang, H.; Duschl, C.; Vogel, H. *Langmuir* **1994**, *10*, 197.
(2) Valincius, G.; Heinrich, F.; Budvytyte, R.; Vanderah, D. J.; Sokolov, Y.; Hall, J. E.; Lösche, M. *Biophys. J.* **2008**, *95*, 4845.
(3) Junghans, A.; Champagne, C.; Cayot, P.; Loupiac, C.; Koper, I. *Langmuir* **2011**, *27*, 2709.
(4) Becucci, L.; Martinuzzi, S.; Monetti, E.; Mercatelli, R.; Quercioli, F.; Battistel, D.; Guidelli, R. *Soft Matter* **2010**, *6*, 2733.
(5) Walz, D.; Bamberg, E.; Läuger, P. *Biophys. J.* **1969**, *9*, 1150.
(6) Weiss, S. A.; Bushby, R. J.; Evans, S. D.; Henderson, P. J. F.; Jeuken, L. J. C. *Biochem. J.* **2009**, *417*, 555.
(7) Danelon, C.; Terrettaz, S.; Guenat, O.; Koudelka, M.; Vogel, H. *Methods* **2008**, *46*, 104.
(8) Song, H.; Sinner, E.-K.; Knoll, W. *Biointerphases* **2007**, *2*, 151.
(9) Zhan, W.; Jiang, K.; Smith, M. D.; Bostic, H. E.; Best, M. D.; Auad, M. L.; Ruppel, J. V.; Kim, C.; Zhang, X. P. *Langmuir* **2010**, *26*, 15671.
(10) Macdonald, J. R.; Johnson, W. B. In *Impedance Spectroscopy Theory, Experiment, and Applications*, 2nd ed.; Barsoukov, E., Macdonald, J. R., Eds.; A John Wiley & Sons, Inc., Publication: Hoboken, NJ, 2005.
(11) Steinem, C.; Janshoff, A.; Galla, H.-J.; Sieber, M. *Bioelectrochem. Bioenerg.* **1997**, *42*, 213.
(12) Vallejo, A. E.; Gervasi, C. A.; Gassa, L. M. *Bioelectrochem. Bioenerg.* **1998**, *47*, 343.
(13) De Levie, R. *Adv. Chem. Phys.* **1978**, *37*, 99.
(14) Vallejo, A. E.; Gervasi, C. A. *Bioelectrochemistry* **2002**, *57*, 1.
(15) Jeuken, L. J. C.; Weiss, S. A.; Henderson, P. J. F.; Evans, S. D.; Bushby, R. J. *Anal. Chem.* **2008**, *80*, 9084.
(16) Redwood, W. R.; Pfeiffer, F. R.; Weisbach, J. A.; Thompson, T. E. *Biochim. Biophys. Acta* **1971**, *233*, 1.
(17) Takashima, S. *Electrical Properties of Biopolymers and Membranes*; Adam Hilger: Bristol and Philadelphia, 1989.
(18) McGillivray, D. J.; Valincius, G.; Vanderah, D. J.; Febo-Ayala, W.; Woodward, T. J.; Heinrich, F.; Kasianowicz, J. J.; Lösche, M. *Biointerphases* **2007**, *2*, 21.
(19) Volkov, A. G.; Paula, S.; Deamer, D. W. *Bioelectrochem. Bioenerg.* **1997**, *42*, 153.
(20) Gurtovenko, A. A.; Anwar, J. *J. Phys. Chem. B* **2007**, *111*, 13379.
(21) Krishna, G.; Schulte, J.; Cornell, B. A.; Pace, R. J.; Osman, P. D. *Langmuir* **2003**, *19*, 2294.

(22) Jenkins, A. T. A.; Bushby, R. J.; Boden, N.; Evans, S. D.; Knowles, P. F.; Liu, Q. Y.; Miles, R. E.; Ogier, S. D. *Langmuir* **1998**, *14*, 4675.
(23) Cornell, B. A.; Braach-Maksvytis, V. L. B.; King, L. G.; Osman, P. D. J.; Raguse, B.; Wieczorek, L.; Pace, R. J. *Nature* **1997**, *387*, 580.
(24) Junghans, A.; Köper, I. *Langmuir* **2010**, *26*, 11035.
(25) Vockenroth, I. K.; Ohm, C.; Robertson, J. W. F.; McGillivray, D. J.; Lösche, M.; Köper, I. *Biointerphases* **2008**, *3*, FA68.
(26) McGillivray, D. J.; Valincius, G.; Heinrich, F.; Robertson, J. W. F.; Vanderah, D. J.; Febo-Ayala, W.; Ignatjev, I.; Lösche, M.; Kasianowicz, J. J. *Biophys. J.* **2009**, *96*, 1547.
(27) De Levie, R. *Electrochim. Acta* **1963**, *8*, 751.
(28) Dicker, D. *SIAM J. Appl. Math.* **1966**, *14*, 1446.
(29) Olver, F. W. J. In *Handbook of Mathematical Functions with Formulas, Graphs, and Mathematical Tables*, 10th ed.; Abramowitz, M., Stegun, I. A., Eds.; National Institute of Standards and Technology: Washington, DC, 1972.
(30) Gabrielli, C. In *Physical Electrochemistry: Principles, Methods, and Applications*, Rubinstein, I., Ed.; Marcel Dekker, Inc: New York, 1995.
(31) Orazem, M.,E.; Tribollet, B. *Electrochemical impedance spectroscopy*; John Wiley & Sons, Inc: Hoboken, NJ, 2008.
(32) Heinrich, F.; Ng, T.; Vanderah, D. J.; Shekhar, P.; Mihailescu, M.; Nanda, H.; Lösche, M. *Langmuir* **2009**, *25*, 4219.
(33) Jeuken, L. J. C.; Connell, S. D.; Henderson, P. J. F.; Gennis, R. B.; Evans, S. D.; Bushby, R. J. *J. Am. Chem. Soc.* **2006**, *128*, 1711.
(34) Valincius, G.; McGillivray, D. J.; Febo-Ayala, W.; Vanderah, D. J.; Kasianowicz, J. J.; Lösche, M. *J. Phys. Chem. B* **2006**, *110*, 10213.
(35) Kwang, K. J.; Valincius, G.; Liao, W.-C.; Hu, X.; Wen, X.; Lee, A.; Yu, B.; Vanderah, D. J.; Lu, W.; Lee, L. J. *Langmuir* **2010**, *26*, 18199.
(36) Lipkowski, J. *Phys. Chem. Chem. Phys.* **2010**, *12*, 13874.
(37) Renner, L.; Pompe, T.; Lemaitre, R.; Drechsel, D.; Werner, C. *Soft Matter* **2010**, *6*, 5382.
(38) Sukhanov, S. V.; Ivanov, B. B.; Orekhov, S. Y.; Barsukov, L. I.; Arseniev, A. S. *Biologicheskie Membrany* **1993**, *10*, 535(in Russian).
(39) Schönknecht, G.; Althoff, G.; Junge, W. *J. Membr. Biol.* **1992**, *126*, 265.
(40) Tao, T.; Xie, J. X.; Drumm, M. L.; Zhao, J. Y.; Davis, P. B.; Ma, J. J. *Biophys. J.* **1996**, *70*, 743.
(41) Knapp, O.; Maier, E.; Mkaddem, S. B.; Benz, R.; Bens, M.; Chenal, A.; Geny, B.; Vandewalle, A.; Popoff, M. R. *Toxicon* **2010**, *55*, 61.
(42) Alahari, A.; Saint, N.; Campagna, S.; Molle, V.; Molle, G.; Kremer, L. *J. Bacteriol.* **2007**, *189*, 6351.
(43) Anzai, K.; Hamasuna, M.; Kadono, H.; Lee, S.; Aoyagi, H.; Kirino, Y. *Biochim. Biophys. Acta* **1991**, *1064*, 256.
(44) Menestrina, G. *J. Membr. Biol.* **1986**, *90*, 177.
(45) Nablo, B. J.; Halverson, K. M.; Robertson, J. W. F.; Nguyen, T. L.; Panchal, R. G.; Gussio, R.; Bavari, S.; Krasilnikov, O. V.; Kasianowicz, J. J. *Biophys. J.* **2008**, *95*, 1157.
(46) Bezrukov, S. M.; Vodyanoy, I.; Brutyan, R. A.; Kasianowicz, J. J. *Macromolecules* **1996**, *29*, 8517.
(47) Korchev, Y. E.; Bashford, C. L.; Alder, G. M.; Kasianowicz, J. J.; Pasternak, C. A. *J. Membr. Biol.* **1995**, *147*, 233.
(48) Knapp, O.; Maier, E.; Masín, J.; Sebo, P.; Benz, R. *Biochim. Biophys. Acta: Biomembr.* **2008**, *1778*, 260.
(49) Beckstein, O.; Sansom, M. S. P. *Phys. Biol.* **2006**, *3*, 147.
(50) Adcock, C.; Smith, G. R.; Sansom, M. S. P. *Eur. Biophys. J. Biophys. Lett.* **2000**, *29*, 29.
(51) Praper, T.; Sonnen, A.; Viero, G.; Kladnik, A.; Froelich, C. J.; Anderluh, G.; Serra, M. D.; Gilbert, R. J. C. *J. Biol. Chem.* **2011**, *286*, 2946.
(52) Meilhac, N.; Destainville, N. *J. Phys. Chem. B* **2011**, *115*, 7190.
(53) Bahrami, A. H.; Jalali, M. A. *J. Chem. Phys.* **2011**, *134*, 085106.
(54) Lang, T.; Rizzoli, S. O. *Physiol. Bethesda Md* **2010**, *25*, 116.
(55) Grage, S. L.; Keleshian, A. M.; Turdzeladze, T.; Battle, A. R.; Tay, W. C.; May, R. P.; Holt, S. A.; Contera, S. A.; Haertlein, M.; Moulin, M.; Pal, P.; Rohde, P. R.; Forsyth, V. T.; Watts, A.; Huang, K. C.; Ulrich, A. S.; Martinac, B. *Biophys. J.* **2011**, *100*, 1252.
(56) Song, L.; Hobaugh, M. R.; Shustak, C.; Cheley, S.; Bayley, H.; Gouaux, J. E. *Science* **1996**, *274*, 1859.
(57) Kendall, J. K. R.; Johnson, B. R. G.; Symonds, P. H.; Imperato, G.; Bushby, R. J.; Gwyer, J. D.; van Berkel, C.; Evans, S. D.; Jeuken, L. J. C. *ChemPhysChem.* **2010**, *11*, 2191.
(58) Vanderah, D. J.; Parr, T.; Silin, V.; Meuse, C. W.; Gates, R. S.; La, H. Y.; Valincius, G. *Langmuir* **2004**, *20*, 1311.
(59) Vanderah, D. J.; Gates, R. S.; Silin, V.; Zeiger, D. N.; Woodward, J. T.; Meuse, C. W.; Valincius, G.; Nickel, B. *Langmuir* **2003**, *19*, 2612.
(60) Lingler, S.; Rubinstein, I.; Knoll, W.; Offenhäusser, A. *Langmuir* **1997**, *13*, 7085.
(61) Whitehouse, C.; O'Flanagan, R.; Lindholm-Sethson, B.; Movaghar, B.; Nelson, A. *Langmuir* **2004**, *20*, 136.
(62) Richter, R. P.; Bérat, R.; Brisson, A. R. *Langmuir* **2006**, *22*, 3497.
(63) Lin, J.; Szymanski, J.; Searson, P. C.; Hristova, K. *Langmuir* **2010**, *26*, 3544.